JOURNAL OF SOLID STATE CHEMISTRY 82, 239–246 (1989)

$M_2VOP_2O_7$ (M = Rb, Cs): Two Vanadyl Pyrophosphates with a Layer Structure

K. H. LII* AND S. L. WANG†

*Institute of Chemistry Academia Sinica, Taipei, Taiwan, Republic of China; †Department of Chemistry, National Tsing Hua University, Hsinchu, Taiwan, Republic of China

Received March 22, 1989; in revised form May 30, 1989

The new compounds $Rb_2VOP_2O_7$ and $Cs_2VOP_2O_7$ were prepared by heating stoichiometric mixtures of Rb_3VO_4 (or Cs_3VO_4), VO_2, V, and P_2O_5 in sealed quartz tubes. For $Rb_2VOP_2O_7$, orthorhombic, $P2_12_12_1$, a = 7.101(1), b = 9.174(2), c = 12.801(4) Å, V = 834.0(4)° Å^3, Z = 4, and R = 5.56%, R_w = 5.88% for 928 independent reflections. For $Cs_2VOP_2O_7$, orthorhombic, $Pnma$, a = 13.280(3), b = 7.247(2), c = 9.518(2) Å, V = 916.0(4) Å^3, Z = 4, and R = 4.12%, R_w = 4.53% for 1118 independent reflections. Both structures consist of corrugated layers of vanadyl pyrophosphate with the alkali metal cations between the layers. Each layer is built up from corner-sharing VO_5 square pyramids and P_2O_7 groups. These two compounds adopt a markedly different structure from $K_2VOP_2O_7$.

Introduction

In 1980, Gorbunova *et al.* (*1*) reported the single-crystal structure of $K_2VOP_2O_7$ which consists of planar layers of vanadyl pyrophosphate with the K^+ cations between the layers. Each potassium ion is coordinated by eight oxygen atoms and the $K^+ \ldots K^+$ distances are 4.00 and 4.34 Å. It would be interesting to know whether there is drastic structural modification if the K^+ cations are fully replaced by the larger cations Rb^+ or Cs^+. As part of a study of the crystal chemistry of early transition metal phosphates, the rubidium and cesium analogues of $K_2VOP_2O_7$ were prepared. The synthesis and crystal structures of the compounds $Rb_2VOP_2O_7$ and $Cs_2VOP_2O_7$ which contain corrugated layers of vanadyl pyrophosphate with the alkali metal cations between the layers are reported.

Experimental

Synthesis

Rb_3VO_4 (99.9%), Cs_3VO_4 (99.9%), VO_2 (99.5%), V (99.5%), and P_2O_5 (99.9%) were purchased from Cerac. Mixtures of M_3VO_4 (M = Rb or Cs), VO_2, V, and P_2O_5 (mole ratio 4 : 1 : 1 : 6) were mixed, pelletized in a nitrogen-filled glove box, and then sealed in evacuated quartz ampoules. Green plate crystals of $Rb_2VOP_2O_7$ for crystal structure analysis were obtained by heating a reaction mixture at 850°C overnight and then furnace-cooled to room temperature. Green plates of $Cs_2VOP_2O_7$ were obtained by heating the reactants at 825°C for 2 hr, slowly cooled to 750°C, maintained at 750°C overnight, and then furnace-cooled to room temperature. Based on visual microscopic examination impurity phases in

0022-4596/89 $3.00

both products were observed. In order to obtain pure $Rb_2VOP_2O_7$ and $Cs_2VOP_2O_7$ for magnetic and spectroscopic studies polycrystalline products were prepared by heating stoichiometric mixtures of the starting materials at 650°C overnight. However, powder X-ray diffraction patterns showed that both products were contaminated with a small amount of unidentified impurities. The strongest reflection of the minor phase in either product was less than 5% of that of the major product.

Single-Crystal X-ray Structure Determination

Two green plate crystals having the dimensions of 0.40 × 0.22 × 0.02 mm for $Rb_2VOP_2O_7$ and 0.35 × 0.35 × 0.08 mm for $Cs_2VOP_2O_7$ were selected for indexing and intensity data collection on a Nicolet R3/V diffractometer. The orientation matrices and unit cell parameters were determined at room temperature by least-squares fit of 22 peak maxima with $10° < 2\theta < 26°$ for $Rb_2VOP_2O_7$ and of 19 peak maxima with $14° < 2\theta < 24°$ for $Cs_2VOP_2O_7$. Corrections for absorption effects were based on ψ scans of a few suitable reflections with χ values close to 90° (*2*). Based on the statistical analysis of the intensity data, the systematic absences, and successful solution and refinement of the structures, the space groups were determined to be $P2_12_12_1$ (No. 19) for the rubidium compound and *Pnma*

TABLE I

SUMMARY OF CRYSTAL DATA, INTENSITY MEASUREMENTS, AND REFINEMENT PARAMETERS FOR $Rb_2VOP_2O_7$ AND $Cs_2VOP_2O_7$

	$Rb_2VOP_2O_7$	$Cs_2VOP_2O_7$
	1. Crystal data	
Space group	$P2_12_12_1$ (No. 19)	*Pnma* (No. 62)
Cell constants	a = 7.101(1) Å	a = 13.280(3) Å
	b = 9.174(2)	b = 7.247(2)
	c = 12.801(4)	c = 9.518(2)
	V = 834.0(4) Å^3	V = 916.0(4) Å^3
Z	4	4
Density (calc, g/cm^3)	3.280	3.674
Abs. coeff. (Mo$K\alpha$)	128.3 cm^{-1}	91.9 cm^{-1}
	2. Intensity measurement	
λ (Mo$K\alpha$)	0.71073 Å	0.71073 Å
Scan mode	$\theta/2\theta$	$\theta/2\theta$
Scan rate	2.93–14.95°/min	2.93–14.95°/min
Scan width	0.96 + $K\alpha_1$, α_2	1.10 + $K\alpha_1$, α_2 separation
Maximum 2θ	55°	60°
Standard reflns	3 every 50	3 every 50 reflns
Unique reflns measured	1154	1436
	3. Structure solution and refinement	
Reflns included	928 ($I > 3\sigma(I)$)	1118 ($I > 3\sigma(I)$)
Parameters refined	119	68
Agreement factors	R = 5.56%, R_w = 5.88%	R = 4.12%, R_w = 4.53%
GOF	1.32	2.28
$(\Delta\rho)_{max}$, $(\Delta\rho)_{min}$	1.33, −1.33 e/Å^3	3.30, −2.60 e/Å^3

(No. 62) for the cesium compound. Both structures were solved by SHELXTL PLUS programs and refined by full-matrix least-squares based on F values. The multiplicities for Rb and Cs were allowed to refine, but did not deviate significantly from full occupancy. Therefore, the alkali metal cations were considered fully occupied in the final cycles of least-squares refinement. Crystal data, intensity measurements, and structure refinement parameters for both structures are listed in Table I. Atomic coordinates and equivalent isotropic thermal parameters are listed in Tables II and III. Selected bond distances and angles are given in Tables IV and V. Tables of observed and calculated structure factor amplitudes and anisotropic thermal parameters are available on request from the authors.

Description of the Structures

$Rb_2VOP_2O_7$. As shown in Fig. 1, the most prominent structural feature of $Rb_2VOP_2O_7$ is the corrugated layers of vanadyl pyrophosphate with the Rb^+ ions between

TABLE II

ATOMIC COORDINATES ($\times 10^4$) AND EQUIVALENT ISOTROPIC DISPLACEMENT PARAMETERS (Å^2 $\times$ 10^2) FOR $Rb_2VOP_2O_7$

	x	y	z	U(eq)
Rb(1)	−2268(2)	−1753(2)	−5947(1)	2.17(4)
Rb(2)	−2697(2)	−3918(2)	−9056(1)	2.04(4)
V(1)	−2481(3)	−2424(2)	−11943(2)	0.98(6)
P(1)	95(4)	−5252(4)	−11510(3)	0.87(8)
P(2)	−848(5)	−109(4)	−8399(3)	1.11(9)
O(1)	−1233(13)	−4341(11)	−12165(9)	1.8(3)
O(2)	−1827(17)	−1935(12)	−10803(9)	2.5(3)
O(3)	−513(15)	−5569(13)	−10415(8)	2.0(3)
O(4)	−540(13)	−1649(10)	−12883(8)	1.7(3)
O(5)	122(14)	−1539(10)	−8174(9)	2.2(3)
O(6)	2004(13)	−4289(10)	−11489(8)	1.3(2)
O(7)	−841(14)	798(11)	−7402(9)	2.3(3)
O(8)	−286(16)	694(15)	−9345(9)	3.0(3)

Note. Equivalent isotropic U defined as one-third of the trace of the orthogonalized U_{ij} tensor.

TABLE III

ATOMIC COORDINATES ($\times 10^4$) AND EQUIVALENT ISOTROPIC DISPLACEMENT PARAMETERS (Å^2 $\times$ 10^2) FOR $Cs_2VOP_2O_7$

	x	y	z	U(eq)
Cs(1)	4010.6(4)	2500	9175.5(6)	2.23(2)
Cs(2)	961.0(4)	2500	1281.2(6)	2.43(2)
V(1)	2873(1)	2500	4868(1)	1.40(4)
P(1)	1582(1)	473(2)	7341(1)	1.24(4)
O(1)	3988(5)	2500	−4519(8)	3.9(3)
O(2)	2209(4)	−653(7)	8366(4)	2.9(1)
O(3)	530(4)	−132(7)	7133(5)	3.4(2)
O(4)	2166(4)	643(6)	−4042(4)	2.6(1)
O(5)	1613(6)	2500	−1954(6)	3.0(2)

Note. Equivalent isotropic U defined as one-third of the trace of the orthogonalized U_{ij} tensor.

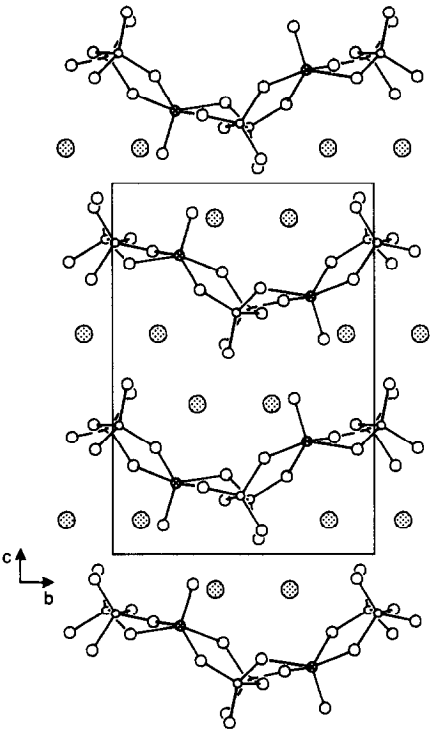

FIG. 1. A projection of the $Rb_2VOP_2O_7$ structure along the a-axis. The Rb, V, P, and O atoms are represented by dotted, cross-hatched, small open, and medium open circules, respectively.

TABLE IV

BOND LENGTHS (Å) AND BOND ANGLES (°) FOR $Rb_2VOP_2O_7$

Bond distances

Rb(1)–O(2*C*)	3.449(12)	Rb(1)–O(3*A*)	2.997(12)
Rb(1)–O(3*D*)	2.849(11)	Rb(1)–O(4*B*)	3.129(10)
Rb(1)–O(5)	3.323(12)	Rb(1)–O(6*B*)	3.458(11)
Rb(1)–O(7)	3.158(11)	Rb(1)–O(8*F*)	2.985(13)
Rb(1)–O(8*C*)	2.857(12)	Rb(2)–O(1*A*)	2.999(11)
Rb(2)–O(2)	2.947(12)	Rb(2)–O(2*B*)	3.041(12)
Rb(2)–O(3)	2.779(11)	Rb(2)–O(4*B*)	3.242(11)
Rb(2)–O(5)	3.169(10)	Rb(2)–O(6*B*)	3.031(10)
Rb(2)–O(7*F*)	3.140(11)	Rb(2)–O(8*B*)	3.198(13)
V(1)–O(1)	1.989(10)	V(1)–O(2)	1.597(12)
V(1)–O(4)	1.963(10)	V(1)–O(5*B*)	1.955(10)
V(1)–O(7*G*)	1.997(11)	P(1)–O(1)	1.514(11)
P(1)–O(3)	1.495(12)	P(1)–O(4*E*)	1.532(10)
P(1)–O(6)	1.619(10)	P(2)–O(5)	1.510(10)
P(2)–O(6*B*)	1.629(10)	P(2)–O(7)	1.524(12)
P(2)–O(8)	1.472(13)		

Bond angles

O(1)–V(1)–O(2)	104.4(5)	O(1)–V(1)–O(4)	85.4(4)
O(2)–V(1)–O(4)	104.7(5)	O(1)–V(1)–O(5*B*)	88.2(4)
O(2)–V(1)–O(5*B*)	108.7(6)	O(4)–V(1)–O(5*B*)	146.5(5)
O(1)–V(1)–O(7*G*)	152.1(5)	O(2)–V(1)–O(7*G*)	103.4(5)
O(4)–V(1)–O(7*G*)	88.2(4)	O(5*B*)–V(1)–O(7*G*)	82.3(4)
O(1)–P(1)–O(3)	116.5(6)	O(1)–P(1)–O(6)	103.2(5)
O(3)–P(1)–O(6)	109.4(6)	O(1)–P(1)–O(4*E*)	108.0(6)
O(3)–P(1)–O(4*E*)	111.9(6)	O(6)–P(1)–O(4*E*)	107.0(5)
O(5)–P(2)–O(7)	108.2(7)	O(5)–P(2)–O(8)	117.9(7)
O(7)–P(2)–O(8)	114.5(7)	O(5)–P(2)–O(6*B*)	98.6(5)
O(7)–P(2)–O(6*B*)	105.2(6)	O(8)–P(2)–O(6*B*)	110.6(6)
P(1)–O(6)–P(2*H*)	126.7(6)		

Symmetry codes

A: $-\frac{1}{2} - x, -1 - y, \frac{1}{2} + z$; *B*: $-\frac{1}{2} + x, -\frac{1}{2} - y, -2 - z$; *C*: $-\frac{1}{2} - x, -y, \frac{1}{2} + z$;
D: $-x, \frac{1}{2} + y, -\frac{3}{2} - z$; *E*: $-x, -\frac{1}{2} + y, -\frac{5}{2} - z$; *F*: $-x, -\frac{1}{2} + y, -\frac{3}{2} - z$;
G: $-\frac{1}{2} - x, -y, -\frac{1}{2} + z$; *H*: $\frac{1}{2} + x, -\frac{1}{2} - y, -2 - z$

the layers. Each layer is built up from corner-sharing VO_5 square pyramids and P_2O_7 groups. Along the *b*-axis the VO_5 square pyramids alternately point up and down relative to a layer. Within a layer heptagonal windows are formed by the edges of three square pyramids and four tetrahedra, but these windows do not form heptagonal tunnels along the *c*-axis (see Figs. 2 and 3). Each VO_5 square pyramid shares its four corners with three P_2O_7 groups with the fifth corner, O(2), being unshared. One of the three P_2O_7 groups acts as a bidentate ligand. The V=O(2) bond length is 1.60(1) Å and is about 0.4 Å shorter than the 4 equatorial V–O bonds, which is a feature characteristic of a VO^{2+} complex. The very short V=O(2) distance is primarily due to the presence of a strong π contribution. The 4 equatorial oxygen atoms are dis-

TABLE V

BOND LENGTHS (Å) AND BOND ANGLES (°) FOR $Cs_2VOP_2O_7$

Bond distances

Cs(1)–O(1*A*)	3.516(8)	Cs(1)–O(2)	3.397(5)
Cs(1)–O(2*G*)	3.397(5)	Cs(1)–O(3*B*)	3.353(5)
Cs(1)–O(3*K*)	3.043(5)	Cs(1)–O(3*C*)	3.353(5)
Cs(1)–O(3*M*)	3.043(5)	Cs(1)–O(4*N*)	3.242(5)
Cs(1)–O(4*E*)	3.242(5)	Cs(1)–O(5*A*)	3.361(8)
Cs(2)–O(5)	3.198(6)	Cs(2)–O(1*D*)	3.111(7)
Cs(2)–O(2*F*)	3.411(5)	Cs(2)–O(2*I*)	3.411(5)
Cs(2)–O(3*J*)	3.024(5)	Cs(2)–O(3*L*)	3.024(5)
Cs(2)–O(4*B*)	3.387(5)	Cs(2)–O(4*C*)	3.387(5)
V(1)–O(1*A*)	1.592(7)	V(1)–O(2*F*)	1.962(5)
V(1)–O(2*I*)	1.962(5)	V(1)–O(4*A*)	1.941(5)
V(1)–O(4*O*)	1.941(5)	P(1)–O(2)	1.520(5)
P(1)–O(3)	1.477(5)	P(1)–O(4*A*)	1.534(4)
P(1)–O(5*A*)	1.616(3)		

Bond angles

O(1*A*)–V(1)–O(2*F*)	108.6(3)	O(1*A*)–V(1)–O(2*I*)	108.6(3)
O(2*F*)–V(1)–O(2*I*)	86.0(3)	O(1*A*)–V(1)–O(4*A*)	104.7(2)
O(2*F*)–V(1)–O(4*A*)	146.7(2)	O(2*I*)–V(1)–O(4*A*)	83.7(2)
O(1*A*)–V(1)–O(4*O*)	104.7(2)	O(2*F*)–V(1)–O(4*O*)	83.7(2)
O(2*I*)–V(1)–O(4*O*)	146.7(2)	O(4*A*)–V(1)–O(4*O*)	87.8(3)
O(2)–P(1)–O(3)	116.4(3)	O(2)–P(1)–O(4*A*)	108.4(3)
O(3)–P(1)–O(4*A*)	112.8(3)	O(2)–P(1)–O(5*A*)	102.0(3)
O(3)–P(1)–O(5*A*)	110.5(4)	O(4*A*)–P(1)–O(5*A*)	105.7(3)
P(1*J*)–O(5)–P(1*H*)	130.8(4)		

Symmetry codes

A: $x, y, 1 + z$; *B*: $\frac{1}{2} - x, \frac{1}{2} + y, \frac{1}{2} + z$; *C*: $\frac{1}{2} - x, -y, \frac{1}{2} + z$;
D: $-\frac{1}{2} + x, y, -\frac{1}{2} - z$; *E*: $\frac{1}{2} - x, -y, \frac{3}{2} + z$; *F*: $\frac{1}{2} - x, \frac{1}{2} + y, -\frac{1}{2} + z$;
G: $x, \frac{1}{2} - y, z$; *H*: $x, \frac{1}{2} - y, -1 + z$; *I*: $\frac{1}{2} - x, -y, -\frac{1}{2} + z$;
J: $-x, -y, 1 - z$; *K*: $\frac{1}{2} + x, \frac{1}{2} - y, \frac{3}{2} - z$; *L*: $-x, \frac{1}{2} + y, 1 - z$;
M: $\frac{1}{2} + x, y, \frac{3}{2} - z$; *N*: $\frac{1}{2} - x, \frac{1}{2} + y, \frac{3}{2} + z$; *O*: $x, \frac{1}{2} - y, 1 + z$

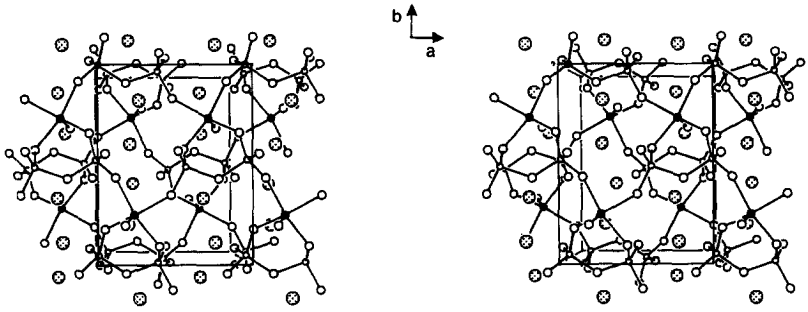

FIG. 2. A stereoscopic view of the $Rb_2VOP_2O_7$ structure along the c-axis. Two successive layers of vanadyl pyrophosphate are shown in this figure.

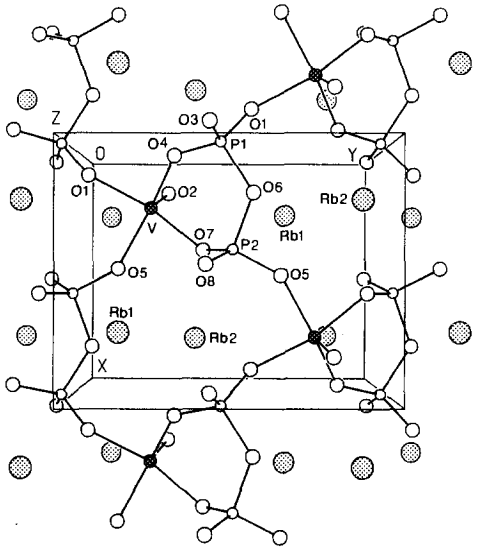

FIG. 3. A layer of vanadyl pyrophosphate in $Rb_2VOP_2O_7$. Positions of the various atoms are indicated.

placed 0.041 to 0.043 Å from the least-squares plane through them. The V^{4+} ion is displaced 0.52 Å from the plane toward the apical oxygen atom O(2). The PO_4 tetrahedra forming the P_2O_7 groups exhibit a semi-eclipsed configuration. The P atom in either tetrahedron shifts away from the bridging oxygen atom, O(6), so that one longer and three shorter P–O bonds are formed. For the three shorter P–O distances, two types of P–O bonds can be distinguished: (i) the shorter bonds P(1)–O(3) and P(2)–O(8) which correspond to the oxygen atoms bonded only to P and Rb atoms; (ii) the longer bonds in which the oxygen atoms are linked to P, Rb, and V atoms. The coordination number of Rb can be determined by the maximum bond distance for Rb–O using the procedure by Donnay and Allmann (*3*) with the revised radii of Shannon (*4*). The two Rb atoms are both bonded to 9 oxygen atoms at distances from 2.85(1) to 3.46(1) Å for Rb(1), and from 2.78(1) to 3.24(1) Å for Rb(2) (see Fig. 4a). The short Rb–O bonds are considerably shorter than the calculated Rb–O distance (3.01 Å) based on Rb^+ (1.63 Å, CN = 9) and O^{2-} (1.38 Å, CN = 4) (*4*). The very short Rb–O bonds involve the oxygen atoms O(3) and O(8) which are linked only to phosphorus and rubidium atoms. The sums of bond strengths are 1.00 and 1.12 for Rb(1) and Rb(2), respectively (*5*). The closest $Rb^+ \ldots Rb^+$ distance is 4.381(3) Å.

$Cs_2VOP_2O_7$. The structure of $Cs_2VOP_2O_7$ is a high-symmetry version of that of $Rb_2VOP_2O_7$. The Cs^+ ions, VO^{2+} complex,

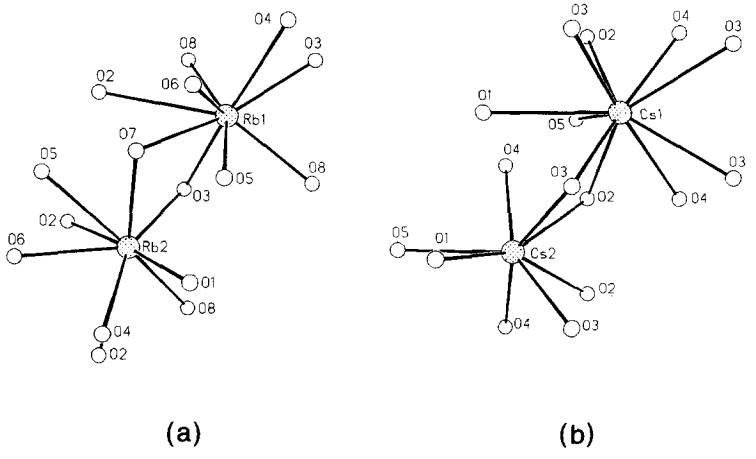

FIG. 4. The coordination of oxygen atoms around Rb and Cs atoms in (a) $Rb_2VOP_2O_7$ and (b) $Cs_2VOP_2O_7$.

and the bridging oxygen atom O(5) in the P_2O_7 group lie in mirror planes perpendicular to the b-axis at $y = \frac{1}{4}$ or $\frac{3}{4}$. Analogous corrugated layers of vanadyl pyrophosphate are also found in the cesium compound (Fig. 5). The heptagonal windows do not form heptagonal tunnels along the a-axis. The connectivity among VO_5 square pyramids and P_2O_7 groups is identical to that in $Rb_2VOP_2O_7$ (Fig. 6). The V–O distances are essentially the same as those in the rubidium compound. The 4 equatorial oxygen atoms in a VO_5 square pyramid lie in a plane and the V^{4+} ion is displaced 0.56 Å toward the apical oxygen atom O(1). The PO_4 tetrahedra in a P_2O_7 group are eclipsed. The P–O bond distances can also be classified into three types: (i) the long bonds (P–O(5)) in which the bridging oxygen atom is shared by two PO_4 tetrahedra; (ii) the intermediate bonds in which the oxygen atoms O(2) and O(4) are bonded to P, Cs, and V atoms; (iii) the short bonds which involve the oxygen atom (O(3)) linked only to Cs and P. Cs(1) is bonded to 10 oxygen atoms at distances from 3.043(5) to 3.516(8) Å, and Cs(2) to 8 oxygen atoms at 3.024(5)–3.411(5) Å, see Fig. 4b. The very short Cs–O bonds also involve the oxygen atom O(3) coordinated only to P and Cs. Bond-strength sums are 1.01 and 0.94 for Cs(1) and Cs(2), respectively. The closest $Cs^+ \ldots Cs^+$ distance is 4.519(1) Å.

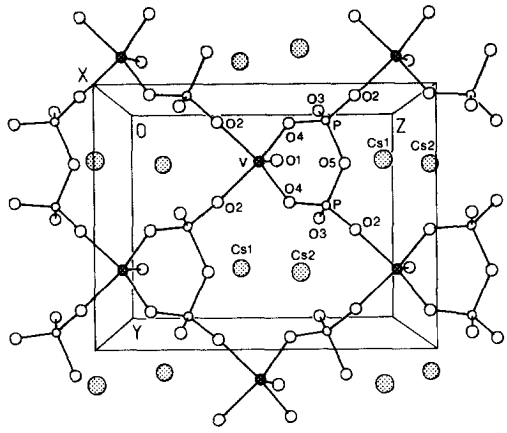

FIG. 6. A layer of vanadyl pyrophosphate in $Cs_2VOP_2O_7$. Positions of the various atoms are indicated.

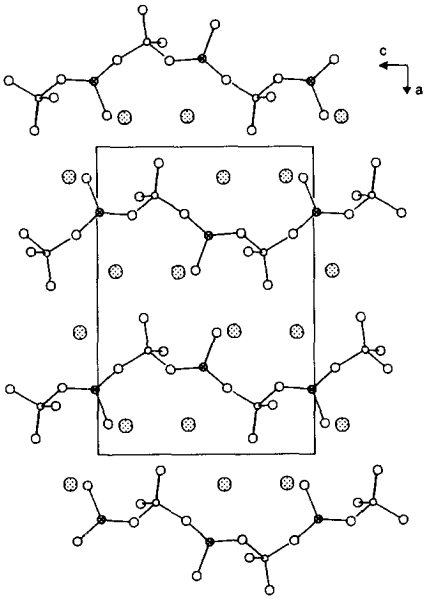

FIG. 5. The unit cell of $Cs_2VOP_2O_7$ as projected down the b-axis. The Cs, V, P, and O atoms are represented by dotted, cross-hatched, small open, and medium open circles, respectively.

Discussion

$K_2VOP_2O_7$ crystallizes in the tetragonal space group $P4bm$ with $a = 8.277(3)$, $c = 5.420(2)$ Å. In $K_2VOP_2O_7$ the connectivity among VO_5 square pyramids and P_2O_7 groups is different from that in $M_2VOP_2O_7$ (M = Cs or Rb). In the potassium compound each VO_5 square pyramid points in one direction and shares its 4 equatorial oxygen atoms with four different P_2O_7 groups. Within a planar layer pentagonal windows are formed by the edges of two square pyramids and three tetrahedra. These windows form pentagonal tunnels parallel to the c-axis. The K^+ ions reside in a mirror plane and the closest $K^+ \ldots K^+$ distance is 4.0 Å, which appears too short for Rb^+ and

Cs^+. A transformation from planar to corrugated layer with concomitant inversion of a half of the VO_5 square pyramids provides a route to accommodate larger cations.

The unit cell volume for $Cs_2VOP_2O_7$ is greater than $Rb_2VOP_2O_7$ by 82 Å^3, which corresponds to 10 Å^3 per alkali metal cation. This volume difference can be compared with that between the cesium and rubidium compounds in the isostructural series $M_4Mo_8P_{12}O_{52}$ (1173 Å^3 for M = Cs, 1134 Å^3 for M = Rb, and 1114 Å^3 for M = K; Z = 1) (*6*). The volume difference between $Rb_4Mo_8P_{12}O_{52}$ and $K_4Mo_8P_{12}O_{52}$ suggests that the unit cell volume for $K_2VOP_2O_7$ would be about 794 Å^3 (Z = 4) if it were isostructural with $Rb_2VOP_2O_7$. Interestingly, $K_2VOP_2O_7$ adopts a markedly different structure with a smaller unit cell volume 371 Å^3, Z = 2) and higher density.

Acknowledgments

Support for this study by the National Science Council and the Institute of Chemistry Academic Sinica is gratefully acknowledged.

References

1. YU. E. GORBUNOVA, S. A. LINDE, A. V. LAVROV, AND I. V. TANANAEV, *Dokl. Akad. Nauk SSSR* **250**(2), 350 (1980).
2. N. W. ALCOCK, *Acta Crystallogr. Sect. A* **30,** 332 (1974).
3. G. DONNAY AND R. ALLMANN, *Amer. Mineral.* **55,** 1003 (1970).
4. R. D. SHANNON, *Acta Crystallogr. Sect. A* **32,** 751 (1976).
5. I. D. BROWN AND D. ALTERMATT, *Acta Crystallogr. Sect. B* **41,** 244 (1985).
6. K. H. LII AND R. C. HAUSHALTER, *J. Solid State Chem.* **69,** 320 (1987).